Plasmonic nanosensor based on Fano resonance in waveguide-coupled resonators

Hua Lu, Xueming Liu,* Dong Mao, and Guoxi Wang

State Key Laboratory of Transient Optics and Photonics, Xi'an Institute of Optics and Precision Mechanics, Chinese Academy of Sciences, Xi'an 710119, China

**Corresponding author: liuxm@opt.ac.cn*

Received June 8, 2012; revised July 31, 2012; accepted August 6, 2012; posted August 7, 2012 (Doc. ID 170212); published September 6, 2012

We propose a plasmonic nanosensor based on Fano resonance in the strong-confinement metal–dielectric–metal waveguide side-coupled with a pair of nanoresonators. Due to the coherent interference of the splitting discrete and quasi-continuum modes, the reflection spectrum possesses a sharp asymmetric Fano resonance dip, which is dependent on the cavity–cavity phase and the refractive index change of the dielectric. The physical features contribute to a highly efficient plasmonic sensor for refractive index sensing. The nanosensor yields a sensitivity of ~900 nm/RIU and a figure of merit of ~500, remarkable values compared with those of plasmonic sensors supported by perfect absorbers.

OCIS codes: 240.6680, 280.4788, 230.4555.

Surface plasmon polaritons (SPPs) have shown the considerable potential to control light at the nanoscale due to their capability to overcome the diffraction limit [1]. Recently, some novel physical features enabling the miniaturization of optical devices have been investigated in various plasmonic nanostructures, such as metamaterials [2,3] and waveguides [1,4,5]. Among these devices, plasmonic sensors for refractive index sensing have been explored by means of the classical analogue of electromagnetically induced transparency (EIT) [2], perfect absorption [3], and so on. A fundamental resonant effect known as Fano resonance, discovered by Ugo Fano, originates from the quantum-mechanical interference between a discrete excited state of an atom and a continuum sharing the same energy level [6,7]. Different from the Lorentzian resonance, the Fano resonance possesses a distinctly asymmetric line profile [8]; asymmetric Fano resonances have been found in classical optical systems [8]. Recently, Fano resonances have been also observed in plasmonic nanostructures, such as nanohole arrays [9], individual coherent plasmonic nanocavities [10], and metamaterials [11]. Fano-like responses can also be designed by deconstructing plasmonic nanoclusters [12,13]. The specific feature of the Fano resonance promises applications in sensors [7]. As an important plasmonic waveguide, metal–dielectric–metal (MDM) configurations attract more and more attention due to their deep-subwavelength confinement of light [4,14–20]. MDM waveguides are regarded as one of the most promising candidates for the nanoscale manipulation and transmission of light [4,14]. MDM waveguide-resonator systems offer a pathway for the realization of photonic functionality in metallic nanostructures [14–20].

In this Letter, we propose and investigate a plasmonic sensor based on Fano resonance in an MDM waveguide-resonator system, which consists of an MDM waveguide side-coupled with a pair of nanoresonators. The theoretical model shows that the Fano resonance lineshape is induced by the splitting resonance modes with different coupling rates and resonance frequencies. The Fano resonance dip strongly relies on the cavity–cavity phase (CCP) and the refractive index of the dielectric. By utilizing the physical features, the nanostructure can work as an excellent plasmonic sensor with a sensitivity of about 900 nm/RIU and a figure of merit (FOM) of about 500.

Figure 1 shows the two-dimensional (2D) schematic diagram of the plasmonic configuration, which consists of an MDM waveguide and two side-coupled nanocavities with length d, width w, and coupling distance g. L and w_c represent the cavity–cavity separation (CCS) and the dielectric thickness of the waveguide, respectively. Here, the metal is assumed as silver, whose permittivity can be determined using the Drude model: $\varepsilon_m(\omega) = \varepsilon_\infty - \omega_p^2/[\omega(\omega + j\gamma)]$ with $\varepsilon_\infty = 3.7$, $\omega_p = 9.1$ eV, and $\gamma = 0.018$ eV [15–17]. For the waveguide-coupled cavity, the localized resonance can be excited when the incident light approaches the intrinsic resonance frequency [14–16]. Similar to other MDM structures, we also focus on the 2D spectral response [14–16,18–20]. The spectral features of waveguide-resonator systems can be investigated by the temporal coupled-mode theory [21]. To simplify the theoretical model, the propagation and coupling losses are not considered. The dielectric in the cavities and waveguide is set as air ($\varepsilon_d = 1$). For the harmonic time dependence of $e^{-j\omega t}$, the time evolution of amplitudes a and b of Cavity A and B can be respectively described as

$$\frac{da}{dt} = (-j\omega_0 - \kappa_0 - \kappa_1)a + e^{j\theta}\sqrt{\kappa_1}S_{+11} + e^{j\theta}\sqrt{\kappa_1}S_{+12}, \quad (1a)$$

$$\frac{db}{dt} = (-j\omega_0 - \kappa_0 - \kappa_1)b + e^{j\theta}\sqrt{\kappa_1}S_{+21} + e^{j\theta}\sqrt{\kappa_1}S_{+22}. \quad (1b)$$

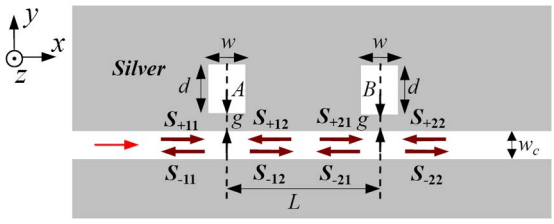

Fig. 1. (Color online) Schematic diagram of the MDM plasmonic dual-resonator-coupled waveguide.

Here ω_0 represents the resonance frequency of cavities. κ_0 is the decay rate of the field due to internal loss in cavities, and κ_1 stands for the decay rate of cavities due to the power escape through the waveguide. These physical parameters are set to be constant with fixed geometrical properties. θ is the phase of coupling coefficient. The outgoing waves of cavities can be expressed as

$$S_{-12} = S_{+11} - e^{-j\theta}\sqrt{\kappa_1}a, \quad S_{-11} = S_{+12} - e^{-j\theta}\sqrt{\kappa_1}a, \quad (2a)$$

$$S_{-21} = S_{+22} - e^{-j\theta}\sqrt{\kappa_1}b, \quad S_{-22} = S_{+21} - e^{-j\theta}\sqrt{\kappa_1}b, \quad (2b)$$

The propagation waves in the waveguide should satisfy the relationship: $S_{+12} = S_{-21}e^{j\varphi}$ and $S_{+21} = S_{-12}e^{j\varphi}$. Here, $\varphi = 2\pi\,\mathrm{Re}(n_{\mathrm{eff}})L/\lambda$ represents CCP of SPP propagation in the waveguide. λ is the incident wavelength in vacuum. n_{eff} is the effective refractive index, which can be achieved by dispersion equations [22]. If the incident light is injected only from the left port ($S_{+22} = 0$), the line shape of the reflection spectrum is expressed as $R = |r|^2 = |S_{-11}/S_{+11}|^2$. The reflection coefficient r can be written as

$$r = e^{j\varphi}(r_1 - r_2), \quad (3a)$$

$$r_1 = \frac{\kappa_1(1 - \cos\varphi)}{j(\Delta\omega - \kappa_1 \sin\varphi) + \kappa_0 + \kappa_1(1 - \cos\varphi)}, \quad (3b)$$

$$r_2 = \frac{\kappa_1(1 + \cos\varphi)}{j(\Delta\omega + \kappa_1 \sin\varphi) + \kappa_0 + \kappa_1(1 + \cos\varphi)}. \quad (3c)$$

Here $\Delta\omega = \omega_0 - \omega$. The reflection coefficient is written as a form of the interference between two new resonance modes with the frequencies of $\omega_0 \pm \kappa_1 \sin\varphi$, coupling decay rates of $\kappa_1(1 \pm \cos\varphi)$, and identical intrinsic decay rates [23]. Figure 2(a) shows the spectral intensities of reflection amplitudes r_1, r_2, and r, which are calculated using the above theoretical modeling with estimated physical parameters obtained by the finite-difference time-domain (FDTD) method. r_1 exhibits a broad bandwidth, which can be regarded as a quasi-continuum. The bandwidth of r_2 is much narrower, which plays the role of a discrete level. The total reflection spectrum possesses asymmetric line profile around the peak of r_2, which is attributed to the coherent interference between r_1 and r_2. The total reflection can be also written as $R = [|r_1|^2 + |r_2|^2 - 2|r_1||r_2|\cos(\theta_2 - \theta_1)]$ [23]. The first two terms stand for the sum of reflection of two resonant modes, and the last term represents the interference between them. Figure 2(b) depicts the phase $\theta_1(\theta_2)$ of $r_1(r_2)$ and their phase difference $\theta_2 - \theta_1$, which depend on the operating wavelength. The total reflection exhibits a sudden drop due to the destructive interference between the two splitting modes when the phase difference $\theta_2 - \theta_1$ approaches zero. The terms $|r_1|^2 + |r_2|^2$ and $-2|r_1||r_2|\cos(\theta_2 - \theta_1)$ are depicted in Fig. 2(c). The interference term exhibits asymmetric profile, which contributes to the asymmetry of total reflection around the Fano resonance dip. As shown in Fig. 2(d), the reflection

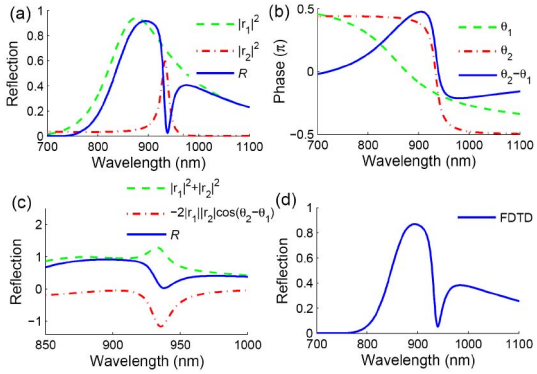

Fig. 2. (Color online) (a) Spectral intensities of r_1 (dashed curve), r_2 (dashed-dotted curve), and r (solid curve). The parameters are estimated as $\omega_0 = 2.076 \times 10^{15}$ rad/s, $\kappa_0 = 5.2 \times 10^{12}$ rad/s, and $\kappa_1 = 1 \times 10^{14}$ rad/s. $L = 400$ nm. (b) Phase term $\theta_1(\theta_2)$ of $r_1(r_2)$ and the phase difference $\theta_2 - \theta_1$. (c) Spectral intensities of $|r_1|^2 + |r_2|^2$, $-2|r_1||r_2|\cos(\theta_2 - \theta_1)$, and R. (d) Reflection spectrum for the structure with $w = 50$ nm, $d = 250$ nm, $g = 5$ nm, and $L = 400$ nm.

in the nanostructure is obtained using the FDTD simulation [24], which is consistent with the theoretical result.

From Eq. (3), it is found that CCP influences the splitting resonant frequencies and the coupling rates and controls the performance of the reflection spectrum. The value of CCP is determined by CCS. Figure 3(a) depicts the reflection spectra with different L obtained by FDTD simulations. We find that the Fano resonance dip disappears in the reflection spectrum when L is changed to 325 nm. The spectrum possesses a peak only at the wavelength of 910 nm. According to the dispersion relation [22], n_{eff} of the waveguide is about 1.392 at 910 nm. Thus, the phase term φ in Eq. (3) is approximately equal to π at 910 nm when $L = 325$ nm. The resonant mode r_2 vanishes. The total reflection $R = |r_1|^2$ and the Fano resonance dip disappear [23]. The Fano resonance dip possesses a redshift around $L = 325$ nm (i.e., $\varphi = \pi$). This is mainly due to the variation of discrete-state resonant mode r_2, whose frequency $\omega = \omega_0 + \kappa_1 \sin\varphi$ decreases with increasing L around the phase $\varphi = \pi$. The

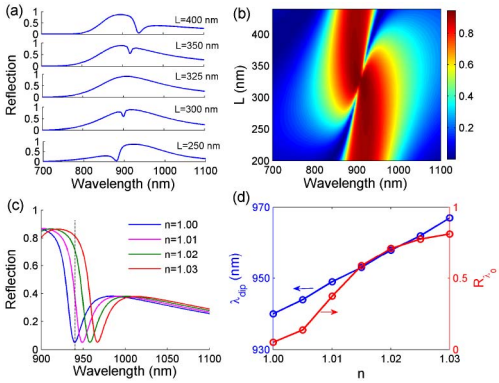

Fig. 3. (Color online) (a) Reflection spectra with different CCS. (b) Evolution of the reflection spectrum with L, which is calculated by the theoretical modeling. (c) Reflection spectra obtained by FDTD simulation for different refractive indices (n) when $L = 400$ nm. (d) Position of the Fano resonance dip as a function of n and the corresponding reflection efficiencies at 940 nm.

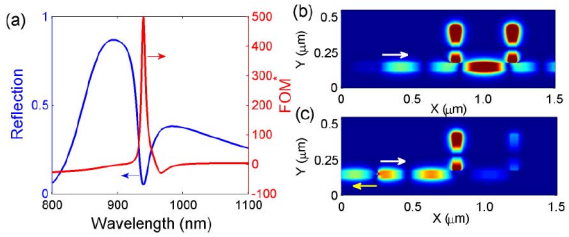

Fig. 4. (Color online) (a) Calculated FOM (red line) and the reflection spectrum with air (blue line). (b) and (c) Field distributions $|H_z|$ with the incident wavelength of 940 nm when $n = 1.00$ (Media 1) and $n = 1.03$ (Media 2). The right and left arrows indicate the incidence and reflection directions, respectively.

simulations agree well with the theoretical results in Fig. 3(b).

The resonance wavelength has a redshift when increasing the refractive index filled in the cavities [15,16]. CCP is also dependent on the effective refractive index, which increases with the refractive index in the waveguide. The resonance wavelength of the splitting mode r_2 increases with the refractive index. Thus, the Fano resonance dip exhibits a sensitive shift with the refractive index change of the dielectric, as seen in Fig. 3(c). This feature provides an excellent scheme for the applications toward nanoscale sensing [2]. The sharp asymmetric Fano line shape enhances the sensitivity of sensors. The sensitivity (nm/RIU) is the shift in the wavelength of the Fano resonance dip per unit change of refractive index (n) [3]. Figure 3(d) reveals that the position of the Fano resonance dip responds linearly to n. The sensitivity is about 900 nm/RIU, which is excellent compared with that of the plasmonic sensors reported [2,3]. For better quantification, the plasmonic sensor detects the relative intensity change dI/I at a fixed wavelength λ_0 induced by a small index change dn. A FOM introduced by Becker *et al.* is defined as $\mathrm{FOM} = \max[dI/(Idn)]$ [25]. Here I represents the average reflection intensity in the waveguide. λ_0 is chosen where the FOM has a maximum [3]. Figure 4(a) depicts the calculated FOM for air with the refractive index change of 0.03 at different wavelengths. The difference between reflection intensities before and after the refractive index change of 0.03 is taken for the derivative, and reflection intensity with $n = 1.00$ is taken for the denominator. The maximum value of the FOM is about 500 at the position of the original Fano resonance dip (i.e., $\lambda_0 = 940$ nm). The FOM is much higher than that of the plasmonic sensors in [3]. Figure 4(b) and 4(c) shows the magnetic field distributions with the incident wavelength of 940 nm before and after the refractive index variation, respectively. It is found that the incident light can pass through the waveguide without reflection, but is reflected when the refraction index is changed to 1.03. The change of the reflection (or transmission) with the refractive index may find other applications in optical switching [18].

In summary, we have proposed a plasmonic nanosensor by means of a Fano resonance in a waveguide-resonator system, which consists of an MDM waveguide side-coupled with a pair of resonators. An obvious Fano resonance dip contributes to the coherent interference of the two splitting resonant modes. One mode with the weak coupling rate plays a role of discrete state, while the other with the strong coupling rate stands for a quasi-continuum. We found that the Fano resonance dip possesses a redshift with increasing CCP around π and is sensitive to the refractive index change of the dielectric. The proposed structure can work as a highly sensitive plasmonic nanosensor with the sensitivity of ~900 nm/RIU and FOM of ~500.

This work was supported by the National Natural Science Foundation of China under Grants 10874239 and 10604066.

References

1. S. I. Bozhevolnyi, V. S. Volkov, E. Devaux, J. Y. Laluet, and T. W. Ebbesen, Nature **440**, 508 (2006).
2. N. Liu, T. Weiss, M. Mesch, L. Langguth, U. Eigenthaler, M. Hirscher, C. Sonnichsen, and H. Giessen, Nano Lett. **10**, 1103 (2010).
3. N. Liu, M. Mesch, T. Weiss, M. Hentschel, and H. Giessen, Nano Lett. **10**, 2342 (2010).
4. P. Neutens, P. Van Dorpe, I. De Vlaminck, L. Lagae, and G. Borghs, Nat. Photonics **3**, 283 (2009).
5. A. Boltasseva, V. Volkov, R. Nielsen, E. Moreno, S. Rodrigo, and S. I. Bozhevolnyi, Opt. Express **16**, 5252 (2008).
6. U. Fano, Phys. Rev. **124**, 1866 (1961).
7. B. Luk'yanchuk, N. Zheludev, S. Maier, N. Halas, P. Nordlander, H. Giessen, and C. Chong, Nat. Mater. **9**, 707 (2010).
8. A. Miroshnichenko, S. Flach, and Y. Kivshar, Rev. Mod. Phys. **82**, 2257 (2010).
9. M. Sarrazin and J. Vigneron, Europhysics News **38**(3), 27 (2007).
10. N. Verellen, Y. Sonnefraud, H. Sobhani, F. Hao, V. Moshchalkov, P. Dorpe, P. Nordlander, and S. Maier, Nano Lett. **9**, 1663 (2009).
11. V. Fedotov, N. Papasimakis, E. Plum, A. Bitzer, M. Walther, P. Kuo, D. P. Tsai, and N. I. Zheludev, Phys. Rev. Lett. **104**, 223901 (2010).
12. M. Rahmani, D. Y. Lei, V. Giannini, B. Lukiyanchuk, M. Ranjbar, T. Liew, M. Hong, and S. Maier, Nano Lett. **12**, 2101 (2012).
13. J. Lassiter, H. Sobhani, M. Knight, W. Mielczarek, P. Nordlander, and N. Halas, Nano Lett. **12**, 1058 (2012).
14. A. Hosseini and Y. Massoud, Appl. Phys. Lett. **90**, 181102 (2007).
15. H. Lu, X. Liu, D. Mao, Y. Gong, and G. Wang, Opt. Lett. **36**, 3233 (2011).
16. H. Lu, X. Liu, D. Mao, L. Wang, and Y. Gong, Opt. Express **18**, 17922 (2010).
17. Z. Han, A. Y. Elezzabi, and V. Van, Appl. Phys. Lett. **96**, 131106 (2010).
18. H. Lu, X. Liu, L. Wang, Y. Gong, and D. Mao, Opt. Express **19**, 2910 (2011).
19. G. Veronis, Z. Yu, Ş. Kocabaş, D. Miller, M. Brongersma, and S. Fan, Chin. Opt. Lett. **7**, 302 (2009).
20. C. Min and G. Veronis, Opt. Express **17**, 10757 (2009).
21. H. A. Haus, *Waves and Fields in Optoelectronics* (Prentice-Hall, 1984) and Chap. 7 within.
22. J. Park, H. Kim, and B. Lee, Opt. Express **16**, 413 (2008).
23. Y. Xiao, M. Li, Y. Liu, Y. Li, X. Sun, and Q. Gong, Phys. Rev. A **82**, 065804 (2010).
24. A. Taflove and S. Hagness, *Computational Electrodynamics: The Finite-Difference Time-Domain Method* 3rd ed. (Artech House, 2005).
25. J. Becker, A. Truegler, A. Jakab, U. Hohenester, and C. Soennichsen, Plasmonics **5**, 161 (2010).